RSC Advances

ROYAL SOCIETY OF CHEMISTRY

www.rsc.org/advances

Graphical Abstract

Preparation of Polypyrrole/Graphene Nanosheets Composites with Enhanced Thermoelectric Properties

Lingyu Wang, Fangzhuan Liu, Cheng Jin, Taoran Zhang and Qinjian Yin*

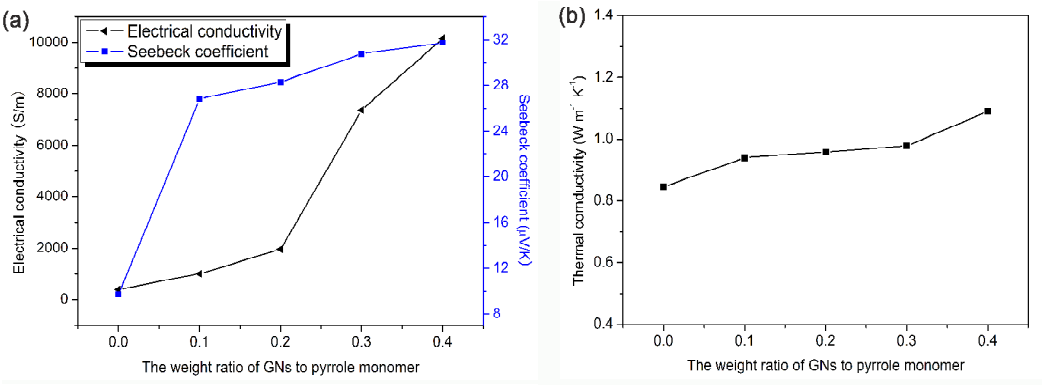

The electrical conductivity and Seebeck coefficient of the PPy/GNs composites have been greatly enhanced as the GNs content increases, while the thermal conductivity still keeps a relatively low value.

RSC Advance

RSCPublishing

ARTICLE

Preparation of Polypyrrole/Graphene Nanosheets Composites with Enhanced Thermoelectric Properties

Cite this: DOI: 10.1039/x0xx00000x

Lingyu Wang, Fangzhuan Liu, Cheng Jin, Taoran Zhang and Qinjian Yin*

Received 00th January 2012,
Accepted 00th January 2012

DOI: 10.1039/x0xx00000x

www.rsc.org/

Polypyrrole/graphene nanosheets (PPy/GNs) composites with enhanced thermoelectric properties have been successfully synthesized by a simple in situ chemical polymerization method with the weight ratio of Py to GNs ranging from 1:0.1 to 1:0.4. FTIR, Raman spectra, SEM and XRD analyses show that strong π-π interactions exist between PPy and GNs, and during polymerization the PPy grew along the surface of the GNs to form a more ordered molecular structure with increased crystallinity. The thermoelectric properties of PPy and PPy/GNs composites were investigated after being cold pressed at room temperature. As the GNs content increases, the Seebeck coefficient could be effectively improved and a remarkably enhanced electrical conductivity has been obtained, while the thermal conductivity of the composites shows no significant change even with high GNs content. As a result, the thermoelectric figure of merit ZT increases with increasing the GNs content and the maximum ZT value of 2.80×10^{-3} is obtained for the composite with the highest GNs content, which is about 210 times higher than that attained from pure PPy. The results of thermogravimetric analysis indicate that the PPy/GNs composites exhibit better thermal stability than pure PPy.

Introduction

Thermoelectric materials that can realize the direct conversion between thermal energy and electrical energy have drawn a lot of attention as a promising candidate to replace traditional carbon-based fossil energy. Thermoelectric materials have wide applications in power generation and energy harvesting, as well as solid state cooling/heating, due to their obvious advantages of functioning without involving any moving parts or hazardous working chemical-fluids.[1, 2] The energy conversion efficiency of thermoelectric materials is evaluated by a dimensionless figure of merit $ZT=S^2\sigma T/\kappa$, where S is the Seebeck coefficient, σ is the electrical conductivity, κ is the thermal conductivity, and T is the absolute temperature.[3] Obviously, a high-performance thermoelectric material is desired for an excellent Seebeck coefficient, a high electrical conductivity, and a low thermal conductivity.[4]

So far, the high performance thermoelectric materials have been mainly focused on inorganic semiconductors and metal alloys, such as Bi_2Te_3, Sb_2Te_3, SiGe and BiSbTe alloys, because of their high power factor.[5-9] But the difficulty in processing and the high cost of raw materials seriously limit their practical applications. In recent years, increasing attention has been paid to organic polymer thermoelectric materials, like polyaniline (PANI), polypyrrole (PPy), and poly(3,4-ethylenedioxythiophene) (PEDOT), due to their increasing figure of merit,[10-13] non-toxicity, flexibility, low cost, potential processing advantages, and especially the low thermal conductivity.[14, 15] However, there is still a big challenge to obtain polymer materials with a simultaneous high electrical conductivity and large Seebeck coefficient.

Graphene, a newly discovered two-dimensional monolayer of sp2-bonded carbon atoms, has received increasing attention in recent years because of its high electrical conductivity, outstanding mechanical properties and thermal conductivity.[16, 17] The researches of polymer-graphene nanocomposites provide a promising way to obtain organic polymer materials with enhanced thermoelectric performance.[18-21] Take PANi/GNs composites for example. It is found that the electrical conductivity and the Seebeck coefficient of PANi/GNs composites are obviously higher than that of the PANi, while the thermal conductivity of the composites still keeps relatively low values even with high GNs content. The highest ZT value is about 70 times higher than that obtained from the PANi.[22]

PPy, among the various conducting materials, has taken special attention because of its low cost, relatively easy processability, high electrical conductivity, and good environmental stability.[23, 24] Based on the above, it is supposed that the PPy/GNs composites would have better thermoelectric performance in comparison with pure PPy. But until now, to the best of our knowledge, there have been many reports about PPy/GNs with improved electrical conductivity and electrochemical properties for the application in energy storage devices,[25-28] while the research on the thermoelectric properties of PPy/GNs composites is very scarce. In this work, a simple in situ chemical polymerization method was employed to prepare the PPy/GNs composites with different GNs contents. The thermoelectric properties of PPy and the PPy/GNs composites

after being cold pressed were investigated at room temperature. It is found that as the GNs content increases, the Seebeck coefficient could be effectively improved and a remarkably enhanced electrical conductivity has been obtained, while the thermal conductivity of the composites shows no significant change even with high GNs content.

Experimental section

Raw materials

Pyrrole (CP, purity ≥ 98.0%) was purchased from Shanghai Kefeng Industry & Commerce Co. Ltd, China and was freshly distilled under vacuum before use. GNs (thickness: < 3 nm, average size: 1-5 μm), were provided by Sichuan Jinlu Group Co.,Ltd, China. Anhydrous ethanol (AR) and $FeCl_3$ $6H_2O$ (AR) were obtained from Chengdu Kelong Chemical Co. Ltd, China and Tianjin Zhiyuan Reagent Co. Ltd, China, respectively. All the reagents were used as received without any further purification except pyrrole. Deionized water was used throughout.

Preparation of PPy/GNs composites

The PPy/GNs composites were prepared by an in situ chemical oxidative polymerization method. In a typical procedure, a designed amount of GNs was first well-dispersed into 100 ml solution (water:ethanol=1:1, v/v) with ultrasonic agitation for 2 h. Then pyrrole monomer (0.0289 mol) was added into the above suspension at 0 ℃-5 ℃ and stirred for 10 min. The mass ratio of pyrrole monomer to GNs was varied as 1:0.1, 1:0.2, 1:0.3, 1:0.4, and the resulting composites were labeled as GP1, GP2, GP3 and GP4, respectively. Afterward, the oxidant solution obtained by dissolving 0.0578 mol $FeCl_3$ $6H_2O$ in 50 ml deionized water was slowly dropped into the above reaction system. Polymerization of pyrrole began in a few minutes. The reaction was carried out under stirring for 24 h at 0 ℃-5 ℃. After the polymerization, the resulting black precipitate was filtered and washed with ethanol and deionized water in sequence for several times. The product thus obtained was dried under vacuum at 60 ℃ overnight. For comparison, pure PPy was also prepared in the absence of GNs using the similar procedure.

Characterization

Fourier transform infrared spectroscopy (FTIR) measurements were conducted on a Bruker Tensor 27 FTIR spectrometer using KBr pellets. Raman spectra were recorded on a Raman spectrometer (Horiba LabRAM HR, Japan) with an excitation wavelength of 532 nm. X-ray diffractometer (XRD, Philips X'Pert-MRD, Netherlands) was employed to study the crystal structure of the powder samples with a scanning rate of 5 °/min from 5 ° to 70 °, using Cu Kα radiation. Thermogravimetric analysis (TG209F1, NETZSCH, Germany) was applied to investigate the thermal stability of the GNs, PPy and PPy/GNs composites under nitrogen flow from 30 ℃ to 800 ℃ at a heating rate of 10 ℃/min. The microstructure of the samples was examined by scanning electron microscopy (SEM, Hitachi S-4800, Japan). For the following investigation of thermoelectric properties, the powder samples were first cold pressed at 45 MPa into a cylinder of 16 mm in diameter and about 3 mm in thickness, and then the obtained pellets were cut carefully into a 3 mm × 3 mm × 15 mm cuboid. For thermal diffusivity measurements, the powder samples were compressed into pellets (12.7 mm in diameter and about 2 mm in thickness) under the same pressure and processing time. The electrical conductivity σ and the Seebeck coefficient S were determined simultaneously at room temperature by the four-probe method on a LINSEIS LSR-3 system. The thermal diffusivity λ was measured by laser flash method (Anter, FL4010) and converted into thermal conductivity according to the equation $\kappa=\lambda d C_p$, where C_p is the specific heat capacity, and d is the density of the pellets.

Results and Discussion

FTIR spectra were used to study the chemical composition of the samples as well as the interactions between PPy matrix and GNs. Fig. 1 presents the FTIR spectra of GNs, PPy and PPy/GNs composites with various GNs contents. For pure PPy, the peaks at 1533 cm^{-1}, 1447 cm^{-1} and 3448 cm^{-1} are attributed to the C-C, C-N and N-H stretching vibration in the pyrrole ring, respectively. The band at 1639 cm^{-1} corresponds to the C=C backbone stretching vibration. The strong peaks at 1162 cm^{-1} and 893 cm^{-1} can describe the doping state of PPy.[24] The peaks located at 1280 cm^{-1} and 1031 cm^{-1} can be assigned to C-N stretching vibrations and C-H in-plane deformation vibrations, respectively.[25] It is worthy of note that the characteristic peak of polypyrrole at 1533 cm^{-1} blueshifts to 1541 cm^{-1} when GNs was introduced into the PPy matrix. The shifting of the peak may be due to the interactions, such as π-π stacking between the surface of GNs and PPy backbone and hydrogen bonding caused by the residual oxygen functional groups on GNs.[27] It proves that PPy has been successfully prepared in the presence of GNs.

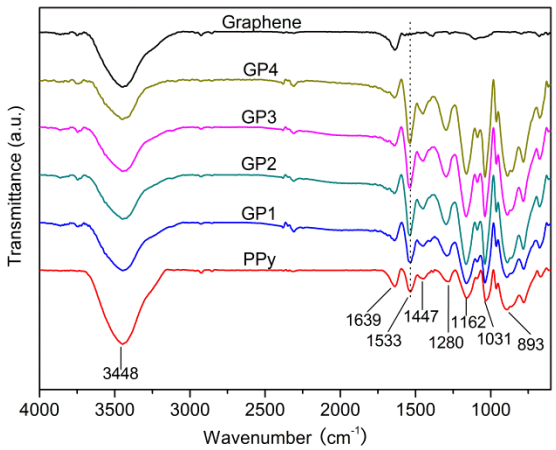

Fig. 1. FTIR spectra of GNs, PPy and PPy/GNs composites with various GNs contents

The interactions between PPy matrix and GNs are further evidenced by Raman spectra, which are depicted in Fig. 2. The Raman spectrum of GNs displays a weak peak at 1346 cm^{-1} and a strong peak at 1580 cm^{-1}, which are attributed to the D band and G band, respectively. The D band corresponds to defects, edge areas or disordered carbon, and the G band is associated with the vibration of sp^2-hybridized carbon.[22, 29] In the spectrum of PPy, only two peaks at 1357 cm^{-1} (D band) and 1568 cm^{-1} (G band) with the similar intensity (I_D/I_G=0.974) are observed, which arise from the ring stretching mode[30] and the C=C backbone stretching vibration of PPy[31], respectively. Nevertheless, the G band of the GP4 composite shifts toward the lower wavenumber to 1562 cm^{-1} compared with pure PPy, which corroborates the π-π interactions between PPy and GNs.[25] This is in line with the FTIR results. Besides, it is found that the intensity ratio of the D band peak to the G band peak (I_D/I_G)

decreases to 0.829 after GNs being loaded, which reveals a decrease in the π-π conjugated defects of the composite compared to pure PPy.

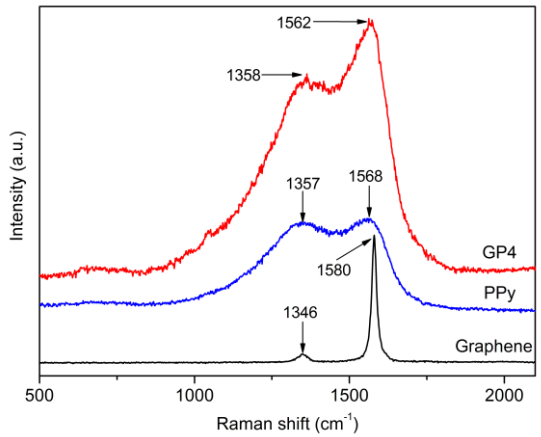

Fig. 2. Raman spectra of GNs, pure PPy and GP4 composite

XRD patterns of the PPy and PPy/GNs composite powders are shown in Fig. 3. For GNs, two diffraction peaks at 2θ = 26.6 ° and 44.1 °corresponds to the graphite-like structure. For pure PPy, only a weak and broad characteristic peak appears at 2θ = 25.9 °, which indicates that pure PPy has an amorphous structure.[31] With increasing the GNs content in the composite, the broad peak becomes narrower and shifts from 2θ = 25.9 ° to 26.3 ° and the peak at 44.1° doesn't obviously appear, indicating that the GNs and PPy have been completely interacted.[27] In addition, there is a significant increase in peak intensity at 26.3 ° with increasing the GNs content and the crystalline character of the composites show an increasing trend as well, which originate from the increasing GNs content.

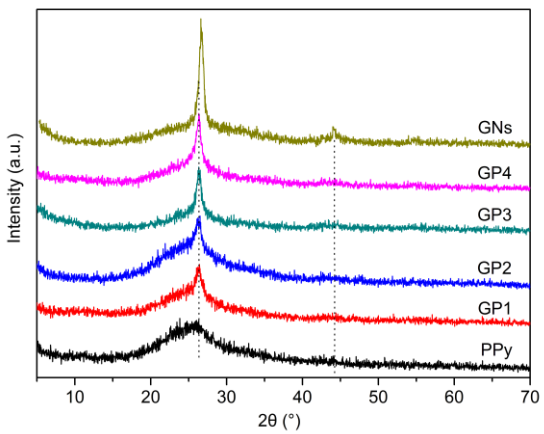

Fig. 3. XRD patterns of PPy and PPy/GNs composites

The thermal stability, which determines the application temperature range, is one of the key parameters for polymer materials. Therefore, TG analysis for the powder samples has been performed under nitrogen flow from 30 ℃ to 800 ℃ and the result is displayed in Fig. 4. The weight loss percentage of the composites are summarized in Table 1. As we can see from Fig. 4 that GNs show an excellent thermal stability even at a high temperature. The weight loss at 800 ℃ is only about 7.1%, which is attributed to its stable 2D structure and the uniform elementary composition with a C/O weight ratio more than 20.[20] In addition, the TGA curves of pure PPy and PPy/GNs composites show a similar shape, suggesting that this samples display a similar degradation procedure. The initial weight loss up to 150℃ may originate from the removal of absorbed water or some volatile impurities.[33] After that, major weight loss takes place, due to the degradation of the PPy chains. However, the PPy/GNs composites exhibit better thermal stability than pure PPy. The residual weight value is found to be increased with increasing the GNs content, probably caused by the following two reasons: One is that the wonderful thermal stability of GNs at a high temperature contributes to the better thermal stability of the composite with higher GNs content; the other is that the mobility and thermal vibration of PPy chains are restricted by the GNs,[34] which would lead to a delay in the degradation of PPy chains.[26]

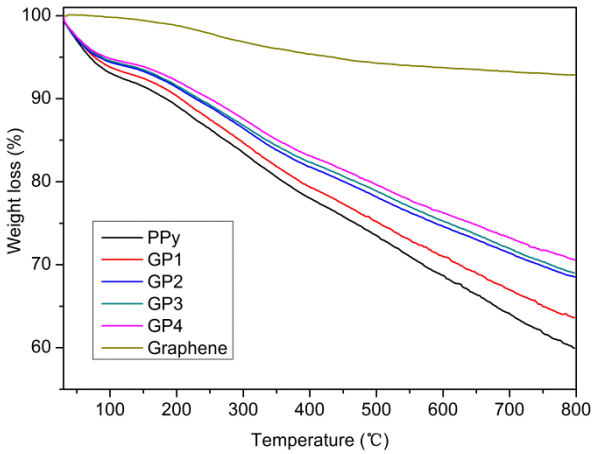

Fig. 4. TGA curves of GNs, PPy and PPy/GNs composites

Table 1 The weight loss percentage of different composites extracted from TGA plots

sample	Weight loss at temperature (%)			
	100 ℃	300℃	600℃	800℃
PPy	6.92	16.5	31.3	40.1
GP1	6.19	15.3	29.1	36.4
GP2	5.60	13.6	25.4	31.5
GP3	5.43	13.2	24.7	30.9
GP4	5.17	12.4	23.7	29.4

Presented in Fig. 5 are the SEM images of GNs, PPy and PPy/GNs composites with different GNs contents. The GNs show a typically curved, sheetlike structure with the average sheet size about 2~5 μm (Fig. 5(a)), which is consistent with the data (1~5 μm) supplied by the manufacturer. The pure PPy exhibits an irregular sphere-like structure with the diameter approximately 300 nm (Fig. 5(b)). As is seen from Fig.5 (c)~(f) that the nanostructure of the PPy depends greatly on the initial weight ratios of pyrrole to GNs. When the weight ratio of pyrrole to GNs is 1:0.1 (Fig. 5(c)), GNs are homogeneously coated with sphere-like PPy particles. As the weight ratio increases to 1:0.2 (Fig. 5(d)), it is interesting to find that on the

GNs surface exist not only sphere-like PPy particles but also rod-like PPy with the diameter about 100~150 nm. The same phenomenon can also be seen in the composites with the weight ratio of 1:0.3 (Fig. 5(e)) and 1:0.4 (Fig. 5(f)). The formation of the PPy nanorods may be attributed to the GNs that acted as the templates in polymerization process. However, the concentration of the GNs when preparing GP1 composite is too low to provide enough templates, and as a result, the PPy in GP1 composite mainly generate spherical particles. In short, the SEM images reveal that the PPy/GNs composites have been successfully prepared via in situ chemical oxidative polymerization with the PPy uniformly coated on the surface of the GNs.

Based on the analysis of the SEM images, a formation mechanism of PPy/GNs composites is put forward in Fig. 6. Firstly, the GNs were well-dispersed into the solution (water:ethanol=1:1, v/v) with ultra-sonication treatment. Secondly, the pyrrole monomer was added into the GNs suspension. Owing to the good solubility of pyrrole in ethanol solution, it is beneficial for pyrrole monomer to uniformly absorb on the surface of GNs through the π-π stacking interaction between the pyrrole ring and the graphene basal planes. But there are still some pyrrole monomers that have not adsorbed on the surface of GNs. The more GNs used, the less the dissociative pyrrole in the reaction system. After the oxidant $FeCl_3$ solution was added, in situ oxidative polymerization of the pyrrole monomer took

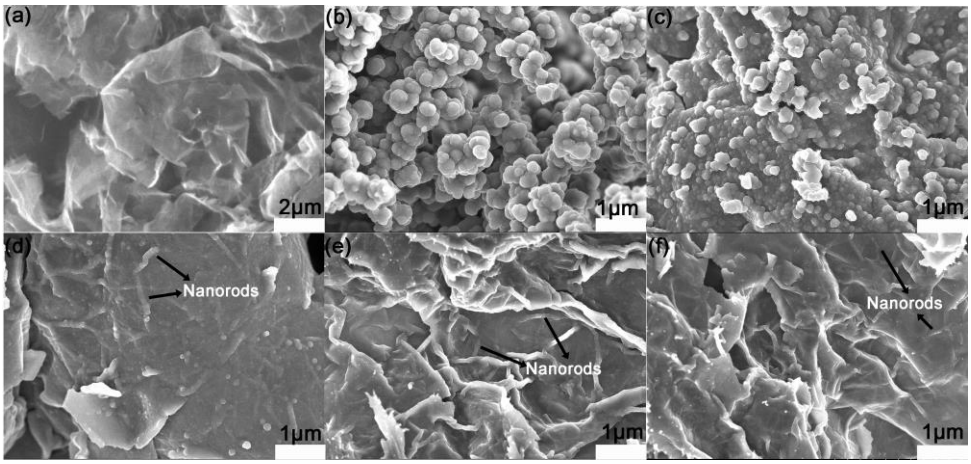

Fig. 5. SEM images of (a) GNs, (b) pure PPy, (c) GP1, (d) GP2, (e) GP3 and (f) GP4

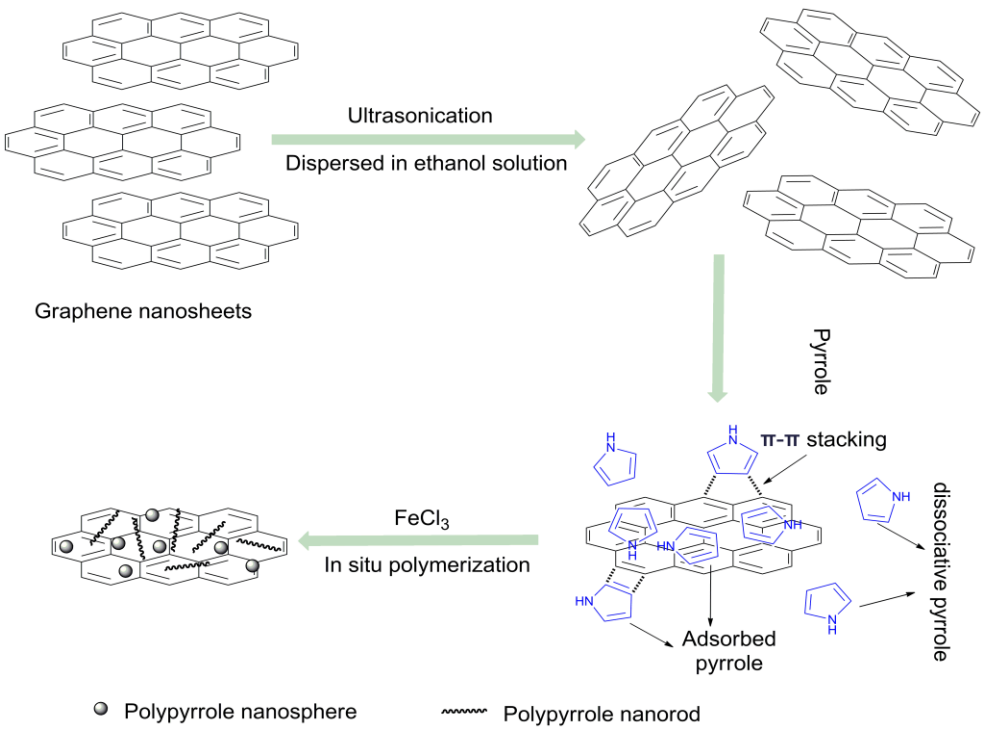

Fig. 6. Schematic illustration of the formation mechanism of PPy/GNs composites

place just from the absorbed sites. When the GNs content is low, the active centers of the polymerization can react not only with the surrounding pyrrole monomer adsorbed on the GNs surface but also with the dissociative pyrrole around. However, when increasing the GNs content, the number of dissociative monomer decreases and thus the active centers have more opportunity to react with the monomer adsorbed on the GNs surface. As a result, the PPy chains in this situation usually grew along the surface of GNs. Therefore, the composites with high GNs content tend to generate PPy nanorods. Consequently, the PPy/GNs composites formed with the GNs uniformly coated by the PPy nanospheres or nanorods.

The room-temperature thermoelectric properties of the PPy/GNs composites are shown in Fig. 7. As we can see from Fig. 7(a) that when the weight ratio of pyrrole to GNs decreases from 1:0.1 to 1:0.4, the electrical conductivity of the composites increases dramatically from 1001 S/m to 10168 S/m. The highest electrical conductivity value of 10168 S/m is about 25.5 times larger than that of pure PPy (~398 S/m). The remarkable electrical conductivity enhancement of the PPy/GNs composites should be attributed to the following two reasons. On one hand, the GNs with excellent electrical conductivity have a homogeneous dispersion in the PPy matrix and more importantly, formed a highly electrically conductive network. On the other hand, the GNs can effectively bridge the carrier transport via the π-π interactions with PPy, which would increase the carrier mobility and thus enhance the electrical conductivity of the PPy/GNs composites.[20, 22]

The Seebeck coefficient of the PPy/GNs composites is also displayed in Fig. 7(a). It is apparent that all the samples exhibit a positive Seebeck coefficient, implying p-type conductive behavior. As the GNs content increases, the Seebeck coefficient has been greatly enhanced from 9.72 μV/K for pure PPy to 31.74 μV/K for the GP4 composite. The enhanced Seebeck coefficient of the composites can be explained by the energy filtering effect at the interfaces between PPy and GNs. The potential boundary barriers at the interfaces would preferentially allow the high-energy carriers to pass, as a result of which, the mean carrier energy in the flow is increased.[32, 35] Accordingly, an increased Seebeck coefficient has received after the GNs were introduced.

Furthermore, it's known that both the electrical conductivity and Seebeck coefficient are largely dependent on the carrier mobility, which can be greatly influenced by the ordering degree of the polymer chains. Highly oriented polymer chains can effectively reduce the barriers of intrachain and interchain hopping and make the carrier move easily.[36, 37] In general, PPy displays a compacted coil conformation and random molecular arrangement. Nevertheless, when GNs were introduced into the polymerization system, PPy was induced to grow along the surface of the GNs via the strong π-π interactions between PPy and GNs. Consequently, PPy formed with the more expanded molecular conformation and more ordered chain packing. This would not only reduce the carrier hopping barrier but also decrease the π-π conjugated defects in the PPy backbone, demonstrated by the Raman spectra. Therefore, the carrier mobility

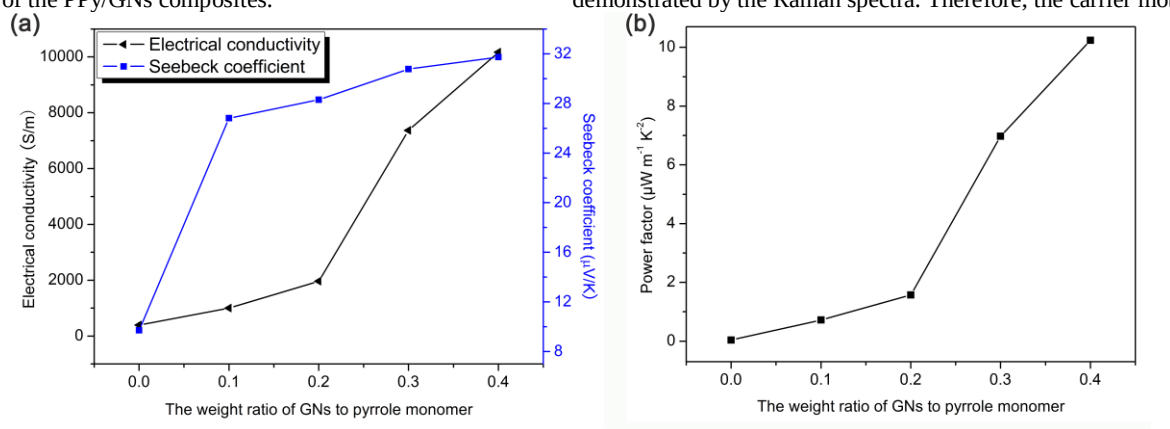

Fig. 7. (a) Electrical conductivity and Seebeck coefficient, and (b) power factor of PPy and PPy/GNs composites at room temperature

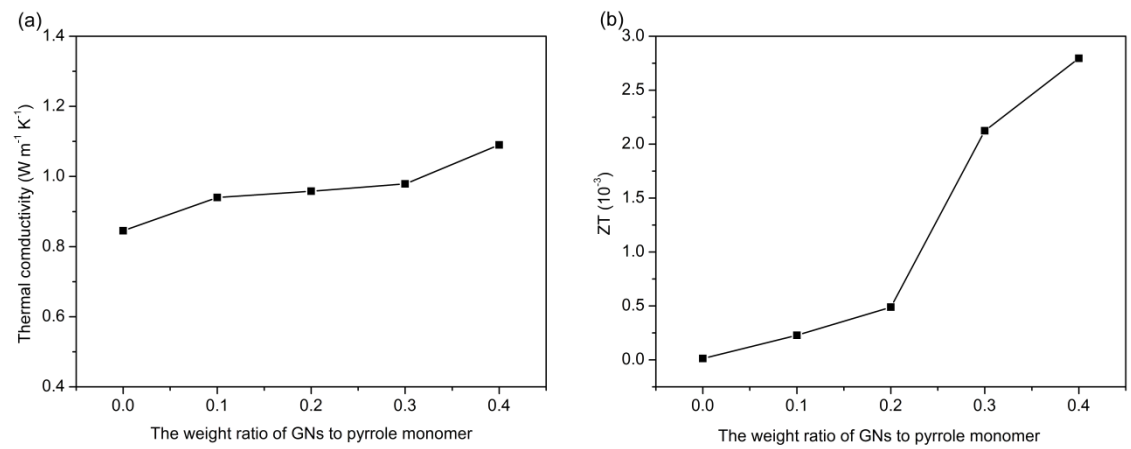

Fig. 8. (a) Thermal conductivity and (b) thermoelectric figure of merit ZT of PPy and PPy/GNs composites at room temperature

is greatly enhanced, further leading to the improvement in both electrical conductivity and Seebeck coefficient.

The calculated power factor ($S^2\sigma$) is shown in Fig. 7(b). Thanks to the simultaneous increase of the electrical conductivity and Seebeck coefficient, an increased power factor has been obtained with increasing the GNs content. The maximum power factor of 10.24 $\mu W\ m^{-1}\ K^{-2}$ for GP4 composite is almost 272 times higher than that of pure PPy (~0.0376 $\mu W\ m^{-1}\ K^{-2}$). In addition, the power factor of the PPy/GNs composites is supposed to be further increased if more GNs are used.

Fig. 8(a) shows the room-temperature thermal conductivity of pure PPy and PPy/GNs composites. Although GNs have an extremely high thermal conductivity, the thermal conductivity of the prepared samples only have a slight increase from 0.84 $W\ m^{-1}\ K^{-1}$ to 1.09 $W\ m^{-1}\ K^{-1}$ with increasing the GNs content, which is still much lower than that of inorganic thermoelectric materials. According to the previous reports, the thermal conductivity for thermoelectric materials originates from both electrons (κ_e) and phonons (κ_p), in which κ_e is proportional to the electrical conductivity.[38] However, the electrical conductivity of PPy and PPy/GNs composites is too low (10^2~10^4 S/m) that the contribution of κ_e to the total thermal conductivity is very small. Therefore, the total thermal conductivity mainly depends on the κ_p. Moreover, previous theoretical and experimental investigations have indicated that nanostructures, including nanointerfaces and nanoinclusions in composites, can efficiently scatter phonons and decrease the κ_p.[35, 39] In the present PPy/GNs composites, between PPy chains and GNs planes form a lot of nanointerfaces, which can act as the excellent scattering centers for phonons, and then reduce the κ_p. Hence, the thermal conductivity of the PPy/GNs composites still keep as low as that of pure PPy, which is beneficial for improving their thermoelectric properties.

The room-temperature ZT values of all the samples are calculated, as shown in Fig. 8(b). The maximum ZT value of 2.80×10^{-3} is obtained for GP4 composites, which is approximately 210 times higher than that of pure PPy. Though the ZT value of 2.80×10^{-3} obtained in this work is among the best levels for conductive polymer-based bulk materials, such as PANi-30GNs composite pellet (ZT_{max} ~1.95×10-3 at 453 K)[22], PANi-50 wt % graphite composite pellet (ZT_{max} ~1.37×10-3 at 393 K)[40], and PANi-41.4 wt % SWNT composite pellet (ZT_{max} ~0.004 at room temperature)[41], there is still much space for further improvement of the thermoelectric performance in comparison with conventional inorganic thermoelectric materials. Finally, optimizing the microstructure and the doping level of polypyrrole may be a promising way to achieve better thermoelectric performance in PPy-based composites.

Conclusions

In this work, PPy/GNs composites have been synthesized at 0~5 ℃ by a simple in situ chemical polymerization method with varying the weight ratio of Py to GNs from 1:0.1 to 1:0.4. In the composites, PPy with a more ordered molecular structure formed along the surface of the GNs, which acted as the templates in the polymerization process to align the PPy chains via the strong π-π interactions between the two components. The simultaneous increase of the electrical conductivity and Seebeck coefficient has been observed in the composites with increasing the GNs content, which stems from the enhanced carrier mobility. Meanwhile, the thermal conductivity of the composites shows no significant change even with high GNs content, and still keeps quite low values, corresponding to the phonon scattering caused by the nanointerfaces in the composites. The highest thermoelectric figure of merit ZT is as high as 2.80×10^{-3}, 210 times higher than that of pure PPy. The results indicate that the low-cost and lightweight PPy/GNs composite has a bright future in thermoelectric applications.

Notes and references

* Key Laboratory of Green Chemistry & Technology, College of Chemistry, Sichuan University, Chengdu 610064, China. Tel: +86 28 85418112; fax: +86 28 85412907; Email: changer@scu.edu.cn

† Footnotes should appear here. These might include comments relevant to but not central to the matter under discussion, limited experimental and spectral data, and crystallographic data.

Electronic Supplementary Information (ESI) available: [details of any supplementary information available should be included here]. See DOI: 10.1039/b000000x/

1. G. J. Snyder and E. S. Toberer, *Nat. Mater.*, 2008, **7**, 105.
2. T. M. Tritt, H. Böttner and L. D. Chen, *MRS Bull.*, 2008, **33**, 366.
3. M. W. Gaultois, T. D. Sparks, C. K. H. Borg, R. Seshadri, W. D. Bonificio and D. R. Clarke, *Chem. Mater.*, 2013, **25**, 2911.
4. M. Zebarjadi, K. Esfarjani, M. S. Dresselhaus, Z. F. Ren and G. Chen, *Energy Environ. Sci.*, 2012, **5**, 5147.
5. M. Scheele, N. Oeschler, K. Meier, A. Kornowski, C. Klinke and H. Weller, *Adv. Funct. Mater.*, 2009, **19**, 3476.
6. G. Q Zhang, B. Kirk, L. A. Jauregui, H. R. Yang, X. F. Xu, Y. P. Chen and Y. Wu, *Nano Lett.*, 2012, **12**, 56.
7. R. C. Jin, G. Chen, J. Pei, H. M. Xu and Z. S. Lv, *RSC Adv.*, 2012, **2**, 1450.
8. H. Lee, D. Vashaee, D. Z. Wang, M. S. Dresselhaus, Z. F. Ren and G. Chen, *J. Appl. Phys.*, 2010, **107**, 4308.
9. T. Zhang, J. Jiang, Y. K. Xiao, Y. B. Zhai, S. H. Yang, G. J. Xu and Z. F. Ren, *RSC Adv*, 2013, **3**, 4951.
10. O. Bubnova, Z. U. Khan, A. Malti, S. Braun, M. Fahlman, M. Berggren and X. Crispin, *Nat. Mater.*, 2011, **10**, 429.
11. T. Park, C. Park, B. Kim, H. Shin and E. Kim, *Energy Environ. Sci.*, 2013, **6**, 788.
12. G-H. Kim, L. Shao, K. Zhang and K. P. Pipe, *Nat. Mater.*, 2013, **12**, 719.
13. R. B. Ašch, N. Blouin, A. Bouchard and M. Leclerc, *Chem. Mater.*, 2009, **21**, 751.
14. M. Hu, D. M. Yu and J. B. Wei, *Polym. Test.*, 2007, **26**, 333.
15. D. M. Price and M. Jarratt, *Thermochim. Acta*, 2002, **392**, 231.
16. X. L. Li, G. Y. Zhang, X. D. Bai, X. M. Sun, X. R. Wang, E. G. Wang and H. J. Dai, *Nat. Nanotechnol.*, 2008, **3**, 538.
17. K. S. Novoselov, A. K. Geim, S. V. Morozov, D. Jiang, Y. Zhang, S. V. Dubonos, I. V. Grigorieva and A. A. Firsov, *Science*, 2004, **306**, 666.
18. Y. Du, S. Z. Shen, W. D. Yang, R. Donelson, K. F. Cai and P. S. Casey, *Synth. Met.*, 2012, **161**, 2688.
19. B. Abad, I. Alda, P. Díaz-Chao, H. Kawakami, A. Almarza, D. Amantia, D. Gutierrez, L. Aubouy and M. Martín-González, *J. Mater. Chem. A*, 2013, **1**, 10450.
20. K. L. Xu, G. M. Chen and D. Qiu, *J. Mater. Chem. A*, 2013, **1**, 12395.
21. Y. Du, K. F. Cai, S. Z. Shen and P. S. Casey, *Synth. Met.*, 2012, **162**, 2102.

22. Y. Lu, Y. Song and F. P. Wang, Mater. *Chem. Phys*., 2013, **138**, 238.
23. L. Li, F. Yan and G. Xue, *J. Appl. Polym. Sci*., 2004, **91**, 303.
24. Z. M. Wu and S-H. Lin, *J. Polym. Sci., Part A: Polym. Chem*., 2006, **44**, 6449.
25. S. Bose, N. H. Kim, T. Kuila, K-T. Lau and J. H. Lee, *Nanotechnology*, 2011, **22**, 295202.
26. Sumanta Sahoo, G. Karthikeyan, Ganesh Ch. Nayak, Chapal Kumar Das. Electrochemical characterization of in situ polypyrrole coated graphene nanocomposites, *Synth. Met*., 2011, **161**, 1713.
27. D. C. Zhang, X. Zhang, Y. Chen, P. Yu, C. H Wang and Y. W. Ma, *J. Power Sources*, 2011, **196**, 5990.
28. S. Biswas and L. T. Drzal, *Chem. Mater*., 2010, **22**, 5667.
29. H. L. Wang, Q. L. Hao, X. J., Yang, L. D. Lu and X. Wang, *Nanoscale*, 2010, **2**, 2164.
30. B. Saner, S. A. Gürsel and Y. Yürüm, *Fullerenes, Nanotubes, Carbon Nanostruct.*, 2013, **21**, 233.
31. Z. M. Gu, C. Z. Li, G. C. Wang, L. Zhang, X. H. Li, W. D. Wang and S. L. Jin, *J. Polym. Sci., Part B: Polym. Phys*., 2010, **48**, 1329.
32. J. Wang, K. F. Cai, S. Shen and J. L. Yin, *Synth. Met*., 2014, **195**, 132.
33. H. Arami, M. Mazloumi, R. Khalifehzadeh, S. H. Emami and S. K. Sadrnezhaad, *Mater. Lett*., 2007, **61**, 4412.
34. K. Lozano and E. V. Barrera, *J. Appl. Polym. Sci*., 2001, **79**, 125.
35. H. J. Song, C. C. Liu, J. K. Xu, Q. L. Jiang and H. Shi, *RSC Adv*., 2013, **3**, 22065.
36. Y. Zhao, G. S. Tang, Z. Z. Yu and J. S. Qi, *Carbon*, 2012, **50**, 3064.
37. Q. Wang, Q. Yao, J. Chang and L. D. Chen, *J. Mater. Chem*., 2012, **22**, 17612.
38. G. D. Mahan and M. Bartkowiak, *Appl. Phys. Lett*., 1999, **74**, 953.
39. A. J. Minnich, M. S. Dresselhaus, Z. F. Ren and G. Chen, *Energy Environ. Sci*., 2009, **2**, 466.
40. L. Wang, D. G. Wang, G. M. Zhu, J. Q. Li and F. Pan, *Mater. Lett*., 2011, **65**, 1086.
41. Q. Yao, L. D. Chen, W. Q. Zhang, S. C. Liufu and X. D. Chen, *ACS Nano*, 2010, **4**, 2445.